Solid Earth Deformations Induced by the Sumatra Earthquakes of 2004-2005: GPS Detection of Co-Seismic Displacements and Tsunami-Induced Loading

H.-P. Plag, G. Blewitt, C. Kreemer, W.C. Hammond
Nevada Bureau of Mines and Geology and Seismological Laboratory, University of Nevada, Reno, Mailstop 178, Reno, NV 89557, USA.

Abstract

The two great Sumatra earthquakes of December 26, 2004, and March 28, 2005, are associated with a number of geodynamic processes affecting Earth's shape, gravity field and rotation on a wide range of spatial and temporal scales. These include co-seismic strong motion, permanent co-seismic displacements, surface loading due to the barotropic tsunami, normal modes, and transient post-seismic deformations lasting from days to years. The December 26, 2004, earthquake is the first one with $M_w > 9.0$ observed with space-geodetic techniques. Thus, new insight into the earthquake processes and associated phenomena can be expected from studies of space-geodetic, and particularly GPS observations. Here we focus on the permanent co-seismic offsets and the tsunami loading signal.

The global patterns of the permanent co-seismic offsets induced by the earthquakes are determined from time series of daily displacements resulting from an analysis of the GPS data from selected stations of the global IGS network. Our estimates are compared to similar estimates computed in other studies. The differences between the independent estimates are mainly noise, and the uncertainties of the offsets are of the order of 2 to 4 mm. The global pattern of the computed offsets is in agreement with the spatial fingerprint predicted by a reasonable rupture model. Using the predicted fingerprint in the determination of the offsets from the GPS time series is expected to improve the estimates of the offsets.

Initial model predictions of the tsunami-induced loading signal show that the peak amplitudes are of the order of 10 to 20 mm. If detectable in GPS time series with low latency, the loading signal could be utilized in a tsunami early warning system.

Keywords: *earthquakes, coseismic displacements, tsunami loading.*

1 Introduction

Great earthquakes like the Sumatra events of 26 December 2004 ($M_w = 9.2$, denoted as "event A") and 28 March 2005 ($M_w = 8.7$, denoted as "event B") are associated with a number of geodynamic phenomena on a wide range of spatial and temporal scales including co-seismic strong motion and permanent displacements, free oscillations of the solid Earth, and, if located in an oceanic region, tsunamis. The redistribution of water masses in the ocean associated with the tsunami induces transient perturbations of the Earth's surface and gravity field. Moreover, post-seismic deformations can continue for months and years after such great earthquakes.

The event A was the first earthquake of $M_w > 9.0$ to be observed with space-geodetic techniques, in particular, the global network of tracking stations for the *Global Positioning System* (GPS), that is coordinated by the *International GNSS Service* (IGS). The expected new insight from studies of the co- and post-seismic displacements into the rupture process of the earthquake and the associated phenomena has stimulated a number of GPS-based studies in the aftermath of the earthquake (e.g. Khan & Gudmundson, 2005; Banerjee et al., 2005; Vigny et al., 2005; Kreemer et al., 2005).

GPS observations potentially provide information on the co-seismic displacements, including the permanent co-seismic offsets, post-seismic non-linear displacements, and tsunami induced loading signals. In order to determine the permanent offset with high accuracy, time series of daily or sub-daily coordinate estimates are required, and these time series also contain the post-seismic signal. For co-seismic oscillations and tsunami-induced loading, time series with high temporal resolution down to 30 sec or better are needed.

The permanent co-seismic offsets are valuable constraints for models of the rupture processes. Moreover, as pointed out by Menke (2005), the magnitudes of earthquakes determined from initial broadband estimates tend to be too low for large earthquakes. This underestimation compromises early warning efforts (Kerr, 2005). Therefore, if available in near-realtime, GPS estimates of the permanent offsets could help to improve the initial magnitude estimates particularly for very large earthquakes. Tsunamis travel the ocean

as barotropic waves and thus induce a loading signal. If detectable by GPS with low latency, these signals could be integrated in an early warning system.

Here, we first consider the permanent co-seismic offsets determined from GPS observations and, by comparing our own estimates to those computed by others, assess the accuracy to which these offsets are determined. Then we will briefly comment on the post-seismic displacements observed at regional stations after the two events.

The surface loading caused by the tsunami is studied on the basis of a model prediction of the sea surface heights variations caused by the tsunami. We use the well validated Green's function approach to estimate the solid Earth deformations induced by the tsunami on the basis of modeled sea surface displacements.

Finally, we will consider the necessary improvements to the observing system and the analysis strategy in order to fully utilize the potential of the GPS (and in the future other Global Navigation Satellite Systems) for studies of large earthquakes and early warning systems.

2 Observed co-seismic surface displacements

In order to determine the permanent co-seismic offset for the two events, GPS data from a total of 39 stations within 7,600 km of the rupture zone (Table 1) were processed for the interval 1 January 2000 to 21 May 2005 using the GIPSY-OASIS II software package from the Jet Propulsion Laboratory (JPL). Daily station cooordinates were estimated using the precise point positioning method (Zumberge et al., 1997) with ambiguity resolution applied successfully across the entire network by automatic selection of the ionospheric- or pseudorange-widelane method (Blewitt, 1989). Satellite orbit and clock parameters, and daily coordinate transformation parameters into ITRF2000 were obtained from JPL. Ionosphere-free combinations of carrier phase and pseudorange were processed every 5 minutes. Estimated parameters included a tropospheric zenith bias and two gradient parameters estimated as random-walk processes, and station clocks estimated as a white-noise process.

For all stations, secular velocities where estimated for the interval 1 January 2000 to 25 December 2004. These velocities are assumed to represent the interseismic tectonic motions prior to event A, and they are used to detrend the data. Moreover, using the stations more than 4000 km away from the epicenter as reference stations, all daily solutions were then transformed by a 7-parameter Helmert transformation onto the constant velocity solution (a process called "spatial filtering").

Table 1: Selected GPS stations used in this study and their nominal distances (D) from the rupture zone. Not all far-field stations are shown.

No.	Stat.	D km	Long. °	Lat. °
1	samp	498	98.72	3.61
2	ntus	1064	103.68	1.35
3	coco	1722	96.83	-12.19
4	bako	1757	106.85	-6.49
5	iisc	2142	77.57	13.02
6	mald	2304	73.53	4.19
7	hyde	2340	78.55	17.42
8	kunm	2605	102.80	25.03
9	dgar	2688	72.37	-7.27
10	lhas	2973	91.10	29.66
11	pimo	3208	121.08	14.64
12	karr	3654	117.10	-20.98
13	wuhn	3711	114.36	30.53
14	tnml	3744	120.99	24.80
15	sey1	4394	55.48	-4.67
16	darw	4440	131.13	-12.84
17	pert	4502	115.89	-31.80
18	kit3	4870	66.89	39.14
19	reun	5003	55.57	-21.21
20	alic	5220	133.89	-23.67
21	bahr	5313	50.61	26.21
22	guam	5677	144.87	13.59
23	lae1	5953	146.99	-6.67
24	tskb	5956	140.09	36.11
25	mali	6047	40.19	-3.00
26	tow2	6281	147.06	-19.27
27	mbar	7072	30.74	-0.60
28	hrao	7841	27.69	-25.89

In Fig. 1, the detrended time series for four stations close to the rupture zones are shown for the interval 1 January 2004 to 21 May 2005. Particularly the sites SAMP and NTUS show large offsets at the time of the two events and significant post-seismic deformations in the months following each of the events. For sites further away, the offsets appear to be hidden in the long-period variations present in the time series. As illustrated by these examples, the determination of the permanent co-seismic offsets is hampered by the presence of noise and other signals in the time series. In particular, it is difficult to estimate reliable errors.

An early analysis of the time series of SAMP and NTUS for event A was presented by Khan & Gudmundson (2005). They used 5 day averages of the north and east displacements to estimate simultaneously a linear trend and the offsets at the time of event A. Their permanent offsets are (given in mm for east, north) $(-145.2 \pm 3.2, -12.1 \pm 1.8)$ and $(-22.0 \pm 2.0, 6.1 \pm 1.6)$ for SAMP and NTUS, respectively.

Banerjee et al. (2005) analysed the data of 41 far-field and regional stations using the GAMIT/GLOBK

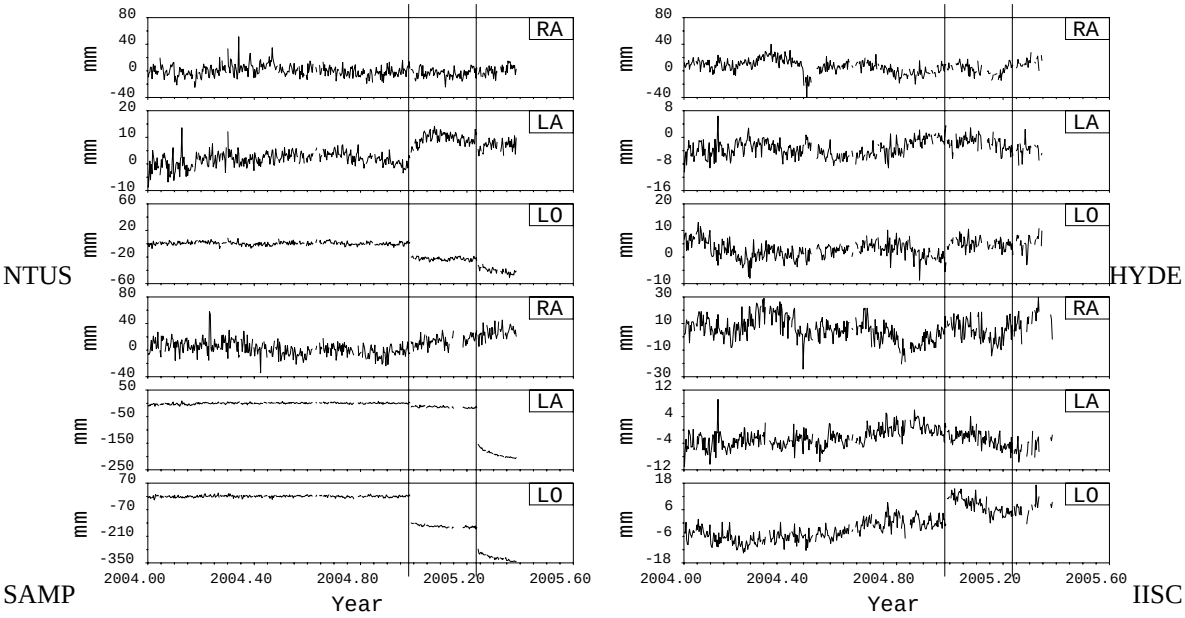

Fig. 1: Detrended displacement time series for permanent GPS sites close to the rupture zone. For each station, the vertical (RA), north (LA) and east (LO) component of the displacement vector are shown. Lower left diagrams are for SAMP, upper left for NTUS, lower right for IISC, and upper right for HYDE. Vertical lines indicate the times of the two events.

software. Permanent offsets for event A were then determined by differencing the mean positions in five days before and after the event A. They claim to see a coherent surface motion for distances up to 4500 km from the epicenter.

Vigny et al. (2005) computed permanent co-seismic offsets from time series of 79 regional and global CGPS sites. These time series were determined using the GIPSY-OASIS II software in precise point positioning mode. The daily solutions for 14 days before and after event A were combined into campaign-like solutions, which were then projected onto ITRF. The offsets were computed as the differences of the 14-day averages after and prior to event A.

Kreemer et al. (2005) using the same time series as in the present study (see above), computed the co-seismic displacements by differencing the average coordinates from 28 days after and before the event. While increasing the span of days before and after the event reduces the noise in the computed average, there is a trade-off with bias from post-seismic displacement, at least for the two stations in the near field of the event (SAMP and NTUS). Therefore, for these two stations, Kreemer et al. (2005) estimated a logarithmic function describing the post-seismic displacements together with the permanent offsets.

The alternative approach chosen here is to model the time series x by the function

$$x(t) = a + bt + \sum_{i=1}^{N_{\mathrm{H}}} \alpha_i H(t_i) + \sum_{j=1}^{N_{\mathrm{C}}} A_j \sin(\omega_j t + \phi_j) \tag{1}$$

where t is time, a is a constant, b a constant rate, and H is a Heaviside function, with α_i giving the displacements associate with event i. We have chosen $N_{\mathrm{H}} = 2$ with the times t_1 and t_2 coinciding with the events A and B, respectively. The harmonic constituents are used to represent a seasonal cycle in the GPS time series, and we have chosen to include an annual and semi-annual constituent (i.e. $N_{\mathrm{C}} = 2$). In the fit, we solve for $a,\ b,\ \alpha_1,\ \alpha_2$ and the amplitudes of the cosine and sine terms of the harmonic constituents. The data prior to approximately December 2002 was found to be of lower quality. Therefore, the data interval for the fit of Eq. 1 to the displacement time series was constrained to 1 January 2003 to 21 May 2005. Examples of the resulting models and the residuals for the stations included in Fig. 1 illustrate that the model function is appropriate for most stations not having significant post-seismic motion (Fig. 2). Particularly for SAMP, the large post-seismic displacement after event B biases the estimated offset for this event if the post-seismic displacement is not modeled properly.

The resulting offset parameters are listed in Table 1. The co-seismic offsets estimated by Banerjee et al.

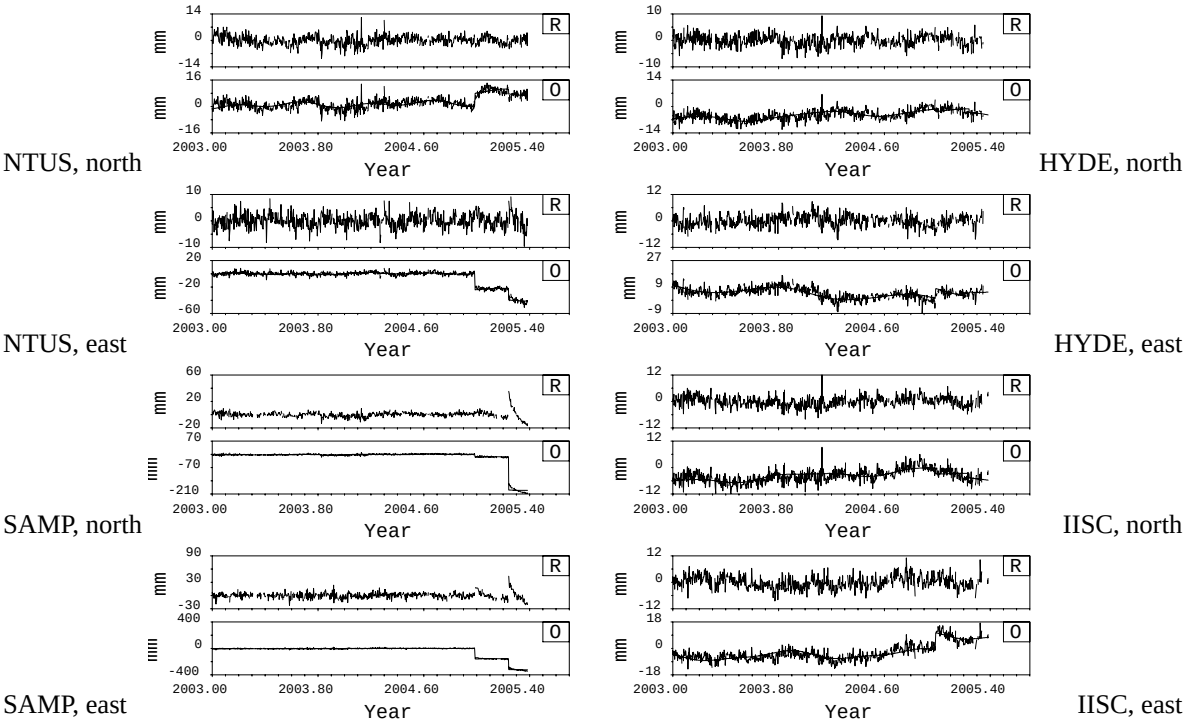

Fig. 2: Determination of co-seismic permanent offsets using eq. (1). Diagrams marked with O show the observations and the model function, while those marked R show the residuals, that is the difference between the observations and the fitted model function.

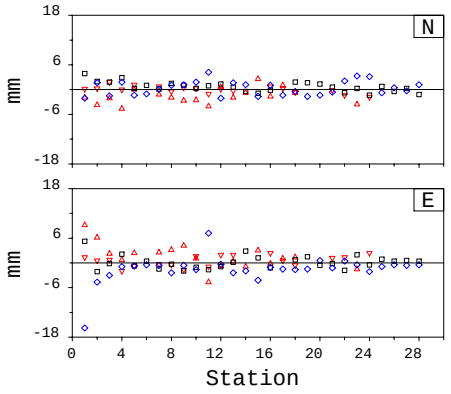

Fig. 3: Comparison of the computed offsets. For each station, the deviation from the mean of all estimates are shown for the east (lower) and north offsets. Triangles: Banerjee et al. (2005), inverted triangles: Vigny et al. (2005), squares: Kreemer et al. (2005), diamonds: this study.

(2005), Vigny et al. (2005) and Kreemer et al. (2005) are also given for comparison. For most stations, the estimates differ by several mm and the error bars do not overlap for all stations. This indicates that the determination of the offsets is not a simple and straight forward process but rather depends on the GPS processing strategy and the model used to approximate the time series prior and after the offsets. The range

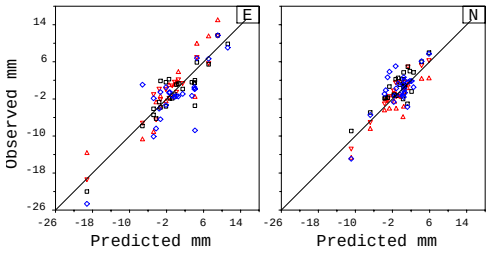

Fig. 5: Comparison of the observed and predicted offsets for event A. Symbols are the same as in Fig. 3.

covered by the four sets of estimates does not appear to depend on the actual offset and there is no clear systematic difference between the four sets (Fig. 3).

Kreemer et al. (2005) computed predicted permanent offsets using a layered elastic spherical Earth model (Pollitz, 1997) and a rupture model that best fits their permanent offsets computed from the GPS series. The predicted displacement field is a dipole with the main motion on both sides of the fracture being directed towards the ruture zone (Fig. 4). Surprisingly large displacements of the order of 5 mm are predicted for areas as far away as South Africa and South America.

The offsets computed in the various studies are in general agreement with the predictions of the model

Table 2: Comparison of permanent co-seismic offsets determined by four independent analyses.

Stat.	Banerjee et al., 2005				Vigny et al., 2005				Kreemer et al., 2005				This study			
	δ_E mm	δ_N mm	σ_E mm	σ_N mm	δ_E mm	δ_N mm	σ_E mm	σ_N mm	δ_E mm	δ_N mm	σ_E mm	σ_N mm	δ_E mm	δ_N mm	σ_E mm	σ_N mm
samp	-135.0	-14.8	6.0	2.2	-142.8	-12.7	3.6	2.0	-139.0	-9.0	1.1	0.6	-160.0	-15.0	0.6	0.6
ntus	-13.8	2.4	3.0	1.6	-19.4	6.4	2.6	1.3	-22.0	8.0	0.6	0.4	-24.6	7.7	0.6	0.6
coco	3.7	1.1	3.4	1.8	2.2	5.0	2.5	2.4	1.3	4.9	0.6	0.4	-1.5	1.6	0.6	0.6
bako	0.9	-3.7	3.6	1.8	-1.7	1.0	4.1	1.9	2.3	3.7	1.3	0.6	-0.7	2.7	0.6	0.6
iisc	14.9	-1.4	2.7	1.5	11.7	-0.1	2.7	2.4	11.7	-1.1	0.6	0.4	11.7	-2.7	0.6	0.6
mald									9.9	4.0	1.1	0.6	9.0	1.9	1.0	1.0
hyde	9.9	-2.7	2.6	1.5	7.0	-0.8	2.5	3.2	5.8	-1.4	0.6	0.4	6.8	-1.4	0.6	0.6
kunm	-2.8	-8.5	3.5	1.8	-6.4	-6.9	3.9	5.1	-6.2	-5.0	1.1	0.6	-8.4	-5.5	0.6	0.6
dgar	11.5	2.2	3.8	2.1	5.7	5.3	3.0	1.7	5.4	6.0	0.6	0.4	6.7	6.1	1.1	1.1
lhas	1.0	-4.2	5.2	2.6	1.7	-1.3	2.5	6.6	-1.1	-1.3	0.8	1.1	-1.6	0.2	0.8	0.6
pimo	-10.8	-4.2	4.0	2.1	-7.1	-1.3	5.4	2.8	-7.9	0.7	0.6	0.6	1.0	3.9	0.4	0.4
karr	-1.8	1.5	3.8	2.1	0.9	1.1	4.4	3.3	-1.9	2.3	0.6	0.4	-1.3	-1.2	0.6	0.6
wuhn	-3.8	-4.5	3.5	2.0	-2.0	-2.9	3.5	4.0	-3.9	-1.9	0.6	0.6	-6.4	-0.9	0.6	0.6
tnml	-9.2	-2.1	3.4	2.0					-5.5	-1.8	0.6	0.4	-10.2	-0.1	0.6	0.6
sey1	-1.6	0.3	7.7	4.3					-3.5	-3.1	0.8	0.4	-8.8	-3.8	0.6	0.6
darw	-2.5	-0.6	4.5	2.3	0.1	1.8	4.9	2.3	-3.6	0.8	0.6	0.4	-3.4	2.0	1.0	1.0
pert	1.8	1.0	1.4	1.3	1.3	0.3	3.8	4.1					-0.8	-1.4	0.6	0.6
kit3	1.6	-1.5	1.8	1.1	-0.4	-1.3	3.3	4.6	1.0	1.1	0.6	0.6	-1.4	-1.1	0.7	0.7
reun									1.6	3.7	1.3	0.6	-1.4	0.5	0.9	0.9
alic									-1.9	1.1	0.4	0.4	-0.6	-1.6	0.6	0.6
bahr					1.5	1.7	8.6	6.7	0.1	2.5	0.4	0.4	-0.9	1.3	0.6	0.6
guam					-1.0	1.6	4.9	2.4	-4.2	2.3	0.6	0.4	-1.9	5.1	0.7	0.7
lae1	-1.5	-6.0	6.6	3.3					1.9	-2.0	0.8	0.6	-0.5	1.0	1.1	1.1
tskb					0.3	-2.3	3.8	3.7	-2.6	-1.8	0.4	0.6	-4.2	2.7	0.6	0.6
mali									2.0	0.7	0.8	0.6	0.1	-0.7	0.8	0.8
tow2									1.6	-0.7	0.6	0.4	0.6	0.3	0.6	0.6
mbar									1.4	0.5	0.6	0.4	0.1	-0.1	1.2	1.2
hrao									1.5	-0.4	0.6	0.6	0.5	1.9	0.7	0.7

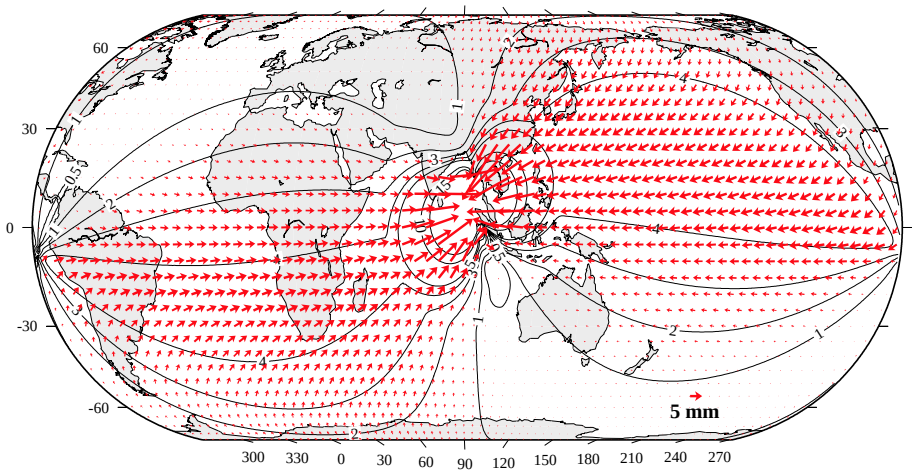

Fig. 4: Predited co-seismic displacement field. The predictions are for a layered elastic spherical Earth model and a rupture model that best fits the offsets computed by Kreemer et al. (2005).

derived by Kreemer et al. (2005) (Fig. 5). Despite the fact that the model is a best fit to the Kreemer et al. (2005) offsets, no systematic differences are detected between the predictions and any of the four sets of estimates. Deviations are generally of the order of a few mm. The estimates for SAMP and NTUS computed by Khan & Gudmundson (2005) fall well into the range covered by the other four estimates.

The largest differences are found for SAMP, where particularly the east offset derived here is biased by the unaccounted post-seismic deformations. For the stations being further than 4000 km away from the rupture zone, the offsets derived here are generally smaller than those determined by Kreemer et al. (2005). Since

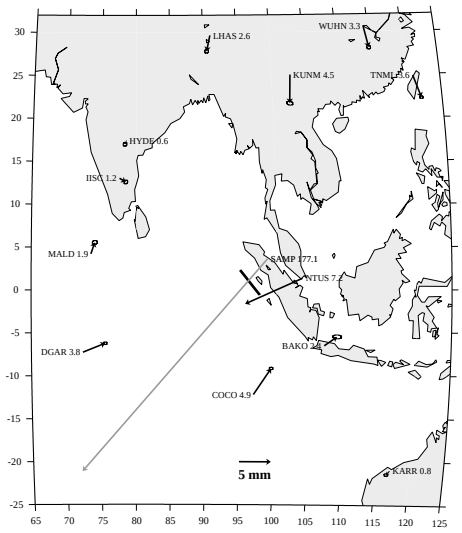

Fig. 6: Co-seismic displacements for Event B. The grey arrow for SAMP is scaled down by a factor of four. The offsets for SAMP and NTUS are determined with the inclusion of the post-seismic deformation term.

these offsets should be close to zero, this may be taken as an indication that using a model function provides slightly better estimates. However, in order to prove this, a more detailed comparison of the observed spatial fingerprint to the predicted fingerprint would be required.

It is emphasized here that Kreemer et al. (2005) used identical time series for the determination of the permanent offsets as the present study but a different approach, while Vigny et al. (2005) used the same software package for the GPS analysis but a different approach to realize the reference frame and to compute the offsets. Banerjee et al. (2005), on the other hand, used time series obtained independently with a different software package. Nevertheless, no systematic differences are found between the Banerjee et al. (2005) and the other estimates.

The comparison of the four sets of estimates reveals that

- the error estimates of Kreemer et al. (2005) and our least squares errors appear to be over-optimistic, while the error estimates of Vigny et al. (2005) and also Banerjee et al. (2005) might be pessimistic;
- the actual uncertainties of the steps are more of the order of 2 to 4 mm;
- only the offsets for stations experiencing displacements larger than a few mm, i.e. if they are in the areas on both sides of the rupture zone, can be determined with statistical significance.

We expect that using the spatial finger-print as predicted by models (see Fig. 4 above) in a multi-station regression for the permanent offsets, will allow a much better determination of the observed displacement field. For that, we suggest a joint regression for the east and north component using the modified model function

$$\vec{x}(t) = a + bt + \sum_{i=1}^{N_\mathrm{P}} \gamma_i \vec{p}_i H(t_i) + \sum_{j=1}^{N_\mathrm{C}} A_j \sin(\omega_j t + \phi_j) \tag{2}$$

to represent the vector of the horizontal components, where $\vec{p}_i$ is the horizontal displacement vector predicted by a rupture model. While the α_i in eq. (1) are the displacements determined independently for each time series, the regression coefficients γ_i are global quantities scaling the model predictions to fit a large number of observed time series without distorting the predicted spatial pattern. Eq. (2), in fact, can be used directly in the search for the best-fit model.

The permanent offsets that can be detected with statistical significance for event B are constrained to relatively few stations (Fig. 6). It is interesting to note that the offset for SAMP is too large to be explained by some kind of dislocation model.

3 Tsunami loading signal

A tsunami travels barotropically through the ocean and causes movements of the ocean water masses comparable to ocean tides. The tsunami similarily loads and deforms the solid Earth. The displacements of the Earth's surface and the changes in the Earth's gravity field induced by surface loads can be computed using the theory of Farrell (1972). Predictions of the perturbations are computed through a convolution of the surface load expressed through the surface pressure and mass density field with the appropriate Green's function.

The initial computations carried out here to estimate the order of magnitude of the induced displacements uses a static Green's function, i.e. the load Love numbers required to compute the Green's functions (see Farrell, 1972, for the details) are calculated neglecting the acceleration term in the field equations for the displacements. Considering that the longest elastic eigenmodes for a non-rotating Earth are of the order of 53 minutes (e.g. Lapwood & Usami, 1981), this static approximation is appropriate for loading with periods of several hours or longer. Tsunamis waves, however, have periods of 30 minutes and less, and the static solution can only give a first order estimate of the amplitude, while arrival times of the loading signal will be

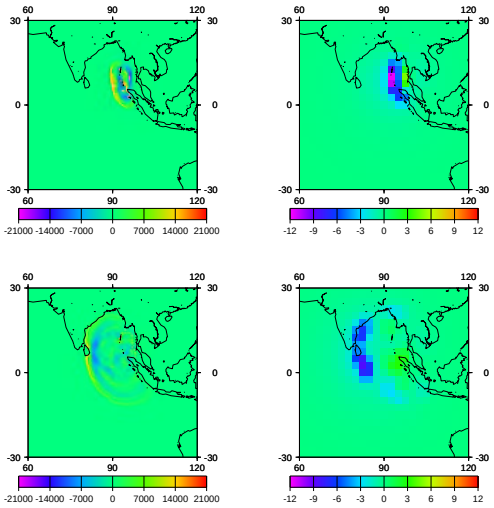

Fig. 7: Ocean bottom pressure and induced vertical displacements computed from predicted sea surface heights. Upper diagrams: 30 minutes after the earthquake, lower diagrams: 2 hours after the earthquake. Left: ocean bottem pressure in Pa; right: vertical displacement of the solid Earth's surface in mm.

strongly biased. Using dynamic Green's function requires not only a convolution in space but also a convolution over the complete history of the tsunami. Thus, for a more accurate modelling of the amplitudes and particularly the temporal variation of the loading signal, a far more complex computation needs to be implemented.

For the tsunami caused by Event A, the surface pressure anomaly, i.e. the ocean bottom pressure variations, are computed from the sea surface height anomalies predicted by the MOST model of the NOAA Tsunami Research Center (Mofjeld et al., 2000). The sea surface heights are given with a mean spatial resolution of $\sim 0.3°$in longitude and $\sim 0.1°$in latitude and a temporal resolution of 5 minutes. For the initial loading computation, a spatial resolution of 2.5 °was used, with the resolution being increased to 0.25 °in coastal areas and close to the observer point.

Shortly after the earthquake the peak deviation in ocean bottom pressure reaches values of more than 200 HPa in the vicinity of the earthquake region (Fig. 7). After two hours, the peak values are still close to 200 HPa with all land areas around the Indian ocean experiencing vertical displacements of the order of 5 to 12 mm (Fig. 7). After nearly a day, the energy of the tsunami has been distributed through a large part of the global ocean, with peak bottom pressure values nearly reaching 10 HPa (Fig. 8). The resulting vertical displacements of the Earth's surface are of the order of

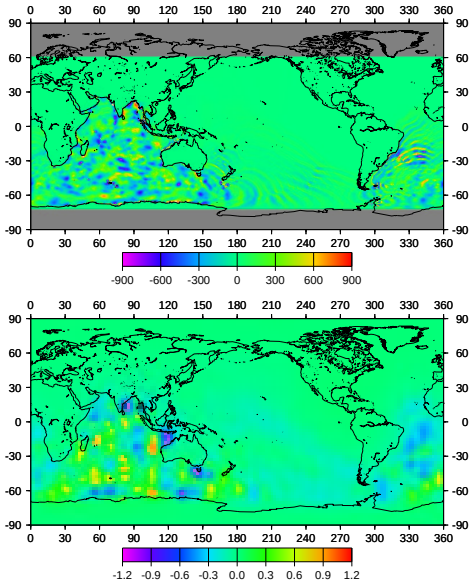

Fig. 8: Same as Figure 7 but for 23 hours after the earthquake.

± 1 mm.

In a detailed search through all loading predictions, peak signals of the order of 20 mm were found in vertical displacements. These peak signals lend to the prospect of detecting tsunami loading using GPS. In particular, the deformational signal with spatial wavelength of the order of 10^2 km should be detectable. However, the processing of GPS observations with high temporal resolution of better than five minutes will have to be improved in order to be able to detect such signals with low latency. In particular, sidereal filtering (Choi et al., 2004) and appropriate regional filtering (Wdowinski et al., 1997, e.g.) will have to be utilized.

4 Conclusions

Event A (26 December 2005) caused the entire Earth surface to deform at a geodetically significant level (> 0.1 mm), with important implications for terrestrial reference frame maintenance. Co-seismic displacements > 2 mm were clearly observed at GPS stations as far away as 4000 km from the rupture zone. The comparison of the co-seismic offsets determined in four different studies shows that the determination of these offsets depends on the GPS analysis as well as the assumptions for the subsequent analysis of the displacement time series. Most of the differences in the calculated offsets appear to be due to noise in the displacements time series. Based on the intercomparison, the uncertainties in the offsets are estimated to be of the order of 2 to 4 mm. Using the spatial fingerprint of

the displacements predicted by realistic rupture models in the estimation of the observed offsets is expected to improve the estimates of the displacement field.

However, a main limitation for the determination of the displacement fields of large earthquakes arises from the number of available permanent GPS sites. At a minimum, attempts should be made to densify the global tracking network in regions with potentially large or great earthquakes to a spatial resolution of 500 km to 1000 km. Combined with models, the stations could be used to determine the effect of these great earthquakes on the global reference frame and to account for it.

The tsunami caused by event A led to transient redistributions of oceanic water masses comparable to those associated with ocean tides. Similar to ocean tidal loading, the tsunami induced displacements of the Earth's surface and gravity changes, with the vertical displacements reaching up to 20 mm. With a sensitive observing system based on e.g. kinematic GPS, these deformations in principle could be sensed in real-time and integrated in a warning system. A similar approaches for storm surge warnings on the basis of tiltmeters was studied by e.g. Kuempel (1983). GPS is far less sensitive to environmental conditions than tilt meters and therefore should sense the tsunami loading signal. However, in order to extract this signal in near-real time, other effects such as the apparent displacements caused by variations in multi-path associated with orbital repetions will have to be reduced sufficiently.

Acknowledgement

The authors are grateful to the International GNSS Service for providing the GPS data, to the IERS for providing reference frame data, and to the Jet Propulsion Laboratory for providing the GIPSY OASIS II software, and precise estimates of satellite orbits, clocks, and reference frame transformations. The sea level height data for the tsunami was made available by Vasily Titov of the NOAA Tsunami Research Center. The work at UNR was funded by grants from NASA Solid Earth and NASA Interdisplinary Science.

References

Banerjee, P., Pollitz, F. F., & Bürgmann, R., 2005. The size and duration of the Sumatra-Andaman earthquake from far-field static offsets, *Science*, **308**, 1769–1772.

Blewitt, G., 1989. Carrier phase ambiguity resolution for the Global Positioning System applied to geodetic baselines up to 2000 km, *J. Geophys. Res.*, **94**(B8), 10187–10283.

Choi, K., Bilich, A., Larson, K. M., & Axelrad, P., 2004. Modified sidereal filtering: Implications for high-rate GPS positioning, *Geophys. Res. Lett.*, **31**, L22608, doi:10.1029/2004GL021621.

Farrell, W. E., 1972. Deformation of the Earth by surface loads., *Rev. Geophys. Space Phys.*, **10**, 761–797.

Kerr, R., 2005. Failure to gauge the quake crippled the warning effort, *Science*, **307**, 201.

Khan, S. A. & Gudmundson, O., 2005. GPS analysis of the Sumatra-Andaman earthquake, *EOS, Trans. Am. Geophys. Union*, **86**, 89–94.

Kreemer, C., Blewitt, G., Hammond, W. C., & Plag, H.-P., 2005. Global deformations from the great 2004 Sumatra-Andaman earthquake observed by GPS: implications for rupture process and global reference frame, *Earth Planets Space*, In press.

Kuempel, H. J., 1983. The possible use of tiltmeters in forecasting storm surges within the German Bay, North Sea, in *Proceedings of the Earth Tide Symposium*, pp. 359–370.

Lapwood, E. & Usami, T., 1981. *Free Oscillations of the Earth*, Cambridge University Press, Cambridge.

Menke, W., 2005. A strategy to rapidly determine the magnitude of great earthquakes, *EOS, Trans. Am. Geophys. Union*, **86**, 185,189.

Mofjeld, H. G., Titov, V. V., Gonzalez, F. I., & Newman, J. C., 2000. Analytic theory of tsunami wave scattering in the ocean with application to the North Pacific ocean, Technical Memorandum OAR PMEL-116, NOAA.

Pollitz, F. F., 1997. Gravitational-viscoelastic postseismic relaxation on a layered spherical Earth, *J. Geophys. Res.*, **102**, 17,921–17,941.

Vigny, C., Simons, W. J. F., Abu, S., Bamphenyu, R., Satirapod, C., Choosakul, N., Subarya, C., Socquet, A., Omar, K., Abidin, H. Z., & Ambrosius, B. A. C., 2005. Insight into the 2004 Sumatra-Andaman earthquake from GPS measurements in southeast Asia, *Nature*, **436**, 201–206.

Wdowinski, S., Bock, Y., Zhang, J., & Fang, P., 1997. Southern California Permanent GPS geodetic array: spatial filterung of daily positions for estimating cosesimic and postseismic displacements induced by the 1992 Landers earthquake, *J. Geophys. Res.*, **102**, 18,057–18,070.

Zumberge, J. F., Heflin, M. B., Jefferson, D. C., & Watkins, M. M., 1997. Precise point positioning for the efficient and robust analysis of GPS data from large networks, *J. Geophys. Res.*, **102**, 5005–5017.